DOI: 10.1002/ ((please add manuscript number))
Article type: Full Paper

Optical Functional Units in Zero-Dimentional Metal Halides as a Paradigm of Tunable Photoluminescence and Multi-Component Chromophores

*Mingze Li, Maxim S. Molokeev, Jing Zhao, Zhiguo Xia**

M. Z. Li, Prof. J. Zhao, Prof. Z. G. Xia
The Beijing Municipal Key Laboratory of New Energy Materials and Technologies, School of Materials Sciences and Engineering, University of Science and Technology Beijing, Beijing 100083, P. R. China
E-mail: xiazg@ustb.edu.cn

Prof. M. S. Molokeev
Laboratory of Crystal Physics, Kirensky Institute of Physics,
Federal Research Center KSC SB RAS,
Krasnoyarsk 660036, Russia

Prof. M. S. Molokeev
Siberian Federal University,
Krasnoyarsk, 660041, Russia

Prof. M. S. Molokeev
Department of Physics,
Far Eastern State Transport University,
Khabarovsk, 680021 Russia

Prof. Z. G. Xia
State Key Laboratory of Luminescent Materials and Devices and Institute of Optical Communication Materials, South China University of Technology, Guangzhou 510641, China
E-mail: xiazg@scut.edu.cn

Keywords: Hybrid metal halides; Structural design; Optical functional applications

Abstract:

Zero-dimensional (0D) organic-inorganic hybrid luminescent metal halides have many promising optoelectronic applications, however, the single building unit in the 0D framework restrict their multi-mode optical control and photoluminescence tuning. Thus, it remains urgent but challenging to rationally design distinct anionic polyhedrons with different optical functions and further expand this family by an equivalent cation substitution and halogen replacement. Herein, $(C_9NH_{20})_9[Pb_3X_{11}](MX_4)_2$ (X = Br and Cl, M = Mn, Fe, Co, Ni, Cu and Zn) have been successfully synthesized verifying the rationality of our design philosophy, and the optical characterizations demonstrate the effects of X-position anions and M-position cations on luminescence process. Intriguingly, both $[Pb_3X_{11}]^{5-}$ and $[MX_4]^{2-}$ perform as inorganic building units in this 0D system and optically active centers, in which the former leads to high-efficiency broad-band yellow/green emission originating from self-trapped excitons and the as-observed multi-component chromophores are derived from the absorption of the latter in the visible light region. Our work highlights the importance of different optical functional units showing synergistic effects on the physical properties and inspires future studies to explore multifunctional application of 0D luminescent metal halides.

1. Introduction

Rational structural design of organic-inorganic hybrid metal halides (OIHMH) attracts increasingly attentions due to their unprecedent structural tunability and excellent optoelectronic properties.[1] For instance, two-dimensional (2D) layered OIHMH can be flexibly designed according to their stacking direction (100)-oriented OIHMH, (110)-oriented OIHMH and (111)-oriented OIHMH) and the numbers of octahedral layers.[2] As a new star material in the OIHMH family, zero-dimensional (0D) OIHMH has received enough interests by their unique 0D structures, however, the structural design of 0D materials is still staying early stage.[3] Selecting appropriate organic ligands and single inorganic building units to form an 0D structure performs as the general principle. However, such a simple design principle quickly encountered its challenge including the limitation of suitable inorganic elements and the monotony of their optical properties. To achieve breakthroughs in material design of 0D OIHMH, several recent studies have been devoted to find mixed 0D systems with two different building units and achieved some exciting achievements. [4] For instance, Han at el. explored a new 0D mixed Bi-Sb OIHMH with ultra-broadband emission,[4a] and Ma discovered a Pb-Zn based 0D material with near-unity PLQY.[4b] Our group also reported a Pb-Mn based 0D compound with tunable emission depending on temperature and excitation wavelength.[4c] Despite this, the rational design principles for this type materials are still vague, and the existed researches appear not to broaden the scope of applications. Thus, designing multiple building units mixed in one lattice

and further expanding the application filed is undoubtedly the next step in the development of new 0D OIHMH systems.

In general, $[PbX_6]^{2-}$, $[SnX_6]^{2-}$ and $[SbX_5]^{2-}$ (X = Cl, Br) are selected as the inorganic parts of 0D OIHMH to exhibit broad-band emission originating from the so-called self-trapped excitons (STEs) or excited-state structural reorganization (ESSR) in some references.[3b, 5] As we know, the conecept of ESSR in 0D system is equivalent as STEs in 2D and 1-dimensional (1D) system, so we use STEs to describe the related photoluminescence process in this work. Owing to the relatively large band gap, most of above materials possess transparent body colors which facilitates their photoluminescence in the visible light region. In contrary, metal halides with building units composed by transitional metal ions (Cr^{3+}, Mn^{2+}, Fe^{2+}, Co^{2+}, Ni^{2+}, Cu^{2+}, etc.) appear various body colors in the visible light region due to their unique electronic transition characteristics. [6] However, these multi-component chromophores and the stable electronic structures make them difficult to form STEs emission as normally observed in other 0D systems. It is anticipated that combining the above two functional units into a single 0D structural framework may create multifunctional materials.

In this work, we propose a widely applicable design principle of 0D OIHMH that allowing two distinct building units with dual-functional properties into a single 0D system, and equivalent cation substitution together with halogen replacement are used to expand this family. Thus, a series of isomorphic 0D materials $(C_9NH_{20})_9[Pb_3X_{11}](MX_4)_2$ (X = Br, Cl, M = Mn, Fe, Co, Ni, Cu, Zn) with two distinct

building units, $[Pb_3X_{11}]^{5-}$ and $[MX_4]^{2-}$, are synthesized as a showcase. We select $[Pb_3X_{11}]^{5-}$ as the fixed component, and typical STEs emission is observed owing to the strong electron-phonon coupling. Simultaneously, $[MX_4]^{2-}$ units with unique absorption characteristics are elected as another variable part, therefore, diverse body colors covering almost the entire visible light region appeared. Multiple optical properties derived from different building units make these materials ideal for multifunctional optical applications. Moreover, detailed characterization and analysis of optical properties revealed the different roles of M-position cations and X-position anions. The newly proposed design principle of multifunctional 0D OIHMH with two different optical functional units undoubtedly create more optical materials with unprecendented multifunctionality.

2. Results and discussion

The simplified schematic diagram (Figure 1a-c) demonstrates the design principle of $(C_9NH_{20})_9[Pb_3X_{11}](MX_4)_2$ (X = Br, Cl, M = Mn, Fe, Co, Ni, Cu, Zn). All of the crystals were prepared by a simple and low-cost solution method, and the synthesis details are shown in the experiment section. As a constant part, $[Pb_3Br_{11}]^{5-}$ clusters as an example consist of three symmetric equivalent $[PbBr_6]^{4-}$ octahedra (Figure 1a). As a variable part, $[MX_4]^{2-}$ can be varied depending on the M-position cations (Figure 1b). The crystal structure of $(C_9NH_{20})_9[Pb_3X_{11}](MX_4)_2$ were finally determined by the correponding single crystal X-ray diffraction (SCXRD) data, which all belong to trigonal system and *P31c* space group. Detailed crystal data and structure refinement were shown in Table S1, and one can also find the crystallographic information files

(CIFs) of the studied compounds $(C_9NH_{20})_9[Pb_3Br_{11}](MBr_4)_2$ (M = Mn, Fe, Co, Ni, Zn) and $(C_9NH_{20})_9[Pb_3Cl_{11}](MCl_4)_2$ (M = Mn, Co, Zn) in the Supporting Information (SI). In addition, simulated and experimental powder X-ray diffraction (PXRD) patterns of $(C_9NH_{20})_9[Pb_3X_{11}](MX_4)_2$ are shown in Figure 1d and Figure 1e to confirm the purity and isomorphism of all the studied metal halide crystals. Moreover, thermogravimetric analysis (TGA) data provided in Figure S1 demonstrate their high chemical stability.

Figure 2a shows optical photographs of $(C_9NH_{20})_9[Pb_3X_{11}](MX_4)_2$ (X = Br, Cl, M = Mn, Fe, Co, Ni, Cu, Zn) crystals under daylight. One can find the all the as-grown crystals possess the large size and high transparency suggesting the ultrahigh crystal quality in our work. Besides, another interesting phenomenon was the variable body colors of different crystals, which suggest that this type materials may find potential applications in multi-functional pigments.[7] The UV-vis reflectance spectra of $(C_9NH_{20})_9[Pb_3X_{11}](MX_4)_2$ samples are depicted in Figure 2b and Figure 2c are used to further understand such an unusual phenomenon. As the M-position cation and X-position anion change as the color tunable chromophores, the clear diversity of the absorption in visible region is observed, which leads to the distinct body colors. Such variable absorption characteristics depending on different transition metal halides are undoubtedly attributed to the different charge transfer transition, in which the X-position anions change the outermost p orbitals of halogens while the M-position cations will alter the 3d orbitals of the transition metals.[6a] In this work, we successfully obtained crystals with different body colors of purple, blue, cyan, green,

yellow, dark yellow, orange, deep red and colorless that containing almost full-region of the visible light, which provide them large potentiality for using in pigment materials.

Figure 3 comparatively demonstrates the photoluminescent properties of the as-grown $(C_9NH_{20})_9[Pb_3Br_{11}](MBr_4)_2$ (M = Mn, Fe, Co, Ni and Zn) and $(C_9NH_{20})_9[Pb_3Cl_{11}](MCl_4)_2$ (M = Mn, Fe Co, Ni, Cu and Zn) crystals, including photoluminescence excitation (PLE) spectra, photoluminescence emission (PL) spectra and photoluminescence decay curves at room temperature (RT). We illustrate all the samples except $(C_9NH_{20})_9[Pb_3Br_{11}](CuBr_4)_2$ since it does not show photoluminescence in the visible light region. As shown in Figure 3a and Figure 3c, samples with the same X-position anion exhibit similar photoluminescence properties. Specifically, Br based samples show broad-band yellow emission peaked at around 565 nm upon the excitation of 365 nm, while Cl based samples can be efficiently excited at 330 nm and show relatively narrower green emission peaking at around 516 nm. The transformation of the M-position cations hardly affect the emission peak, which make it easy for us to attribute the emission center to the $[Pb_3X_{11}]^{5-}$ clusters. Moreover, Figure 3b and Figure 3d show the decay curves of $(C_9NH_{20})_9[Pb_3Br_{11}](MBr_4)_2$ and $(C_9NH_{20})_9[Pb_3Cl_{11}](MCl_4)_2$, respectively, and the nanosecond lifetime is consistent with other Pb-based hybrid halides.[8] The above optical parameters demonstrate that the emission of $(C_9NH_{20})_9[Pb_3X_{11}](MX_4)_2$ is derived from the contrubtion of $[Pb_3X_{11}]^{5-}$ part, and the typical STEs mechanism can be well-explained for the broadband emission (FWHM ~75 nm for Br based samples

and ~61 nm for Cl based samples) and large Stokes shift (~200 nm for Br samples and ~186 nm for Cl samples).[9] It must be pointed out that there is a special compound among the following materials, $(C_9NH_{20})_9[Pb_3Br_{11}](MnBr_4)_2$, which has an extra emission band under 450 nm excitation and thus forms multiple-emission. The PLE and PL spectra of $(C_9NH_{20})_9[Pb_3Br_{11}](MnBr_4)_2$ with excitation wavelength of 450 nm and emission wavelength of 528 nm is provided in Figure S2. The green emission peaked at 528 nm with the FWHM of 67 nm is undoubtedly attributed to the $^4T_1$-$^6A_1$ transition of Mn^{2+} ions, and the long millisecond lifetime (Figure S3) further confirm this hypothesis.[10] More detailed photophysical analysis about $(C_9NH_{20})_9[Pb_3Br_{11}](MnBr_4)_2$ can be found in our recent work.[4c]Such multiple-emission mechanism also provides more application prospects for halide compounds with simultaneously multiple halometalate anions.

Although the above spectral analysis determines that the $[Pb_3X_{11}]^{5-}$ clusters are mainly responsible for the broadband yellow/green emission, however, there are still two issues that should be explained: (1) How does the different X-position anions affect the luminescence? (2) In the situation of the same X-position anions, does different M-position cations also have an influence on the emission? Therefore, a careful comparison of the photophysical properties of all samples is necessary. Firstly, the PLE/PL peak of the Cl based samples have a significant blue shift compared to the Br based samples, which can be attributed to the excited states with higher energy of Cl based halides.[11] In addition, as shown in Figure 4a and Figure 4b, Cl based samples possess higher PLQY (MnCl sample and ZnCl sample even reached

near-unity PLQY) and longer photoluminescence decay time, which is probably corresponding to the different emission quenching temperature defined by the energy barrier for the non-radiative decay.[5a,12] Thus, the quenching temperature of Cl-based compounds is quite higher than that of Br-based samples and thus display higher PLQY and longer lifetime at room temperature. As for the possible effect of M-position cations, we also compared the PLQY (Figure 4a) and photoluminescence decay time (Figure 4b) with the variation of M cations. Interestingly, the results show significant disparity though the samples possess similar PLE/PL spectra, in which Mn based samples and Zn based samples have much higher PLQY and longer photoluminescence decay time compared with other samples. The results can be reasonably explained by combining with previous diffuse reflectance data: Mn based and Zn based samples have almost no absorption in the visible light region, in that case the fluorescence will not be affected by the absorption of the material itself; In contrary, other samples all possess relatively stronger absorption in the emission region (450 nm – 650 nm), so the self-absorption can partially quench the emission through a fast pathway of de-trapping from STEs to the d level of M^{2+} cation. In this case, Fe, Co, Ni, Cu based samples possess relatively low PLQY and short life time. One of the most extreme examples of self-absorption is $(C_9NH_{20})_9[Pb_3Br_{11}](CuBr_4)_2$, which abosorbs almost all the visible light from 450 nm to 700 nm and therefore exhibt invisible emission.

Excitation power dependent PL spectra of the selected samples (Figure S4) were measured and used to exclude the effect of permanent defects which may also cause

the fluorescent emissions in 0D OIHMH.[13] As shown in Figure 4c and Figure 4d, linear relationship between emission intensity and excitation power confirm that the broad-band yellow/green emission is not originated from permanent defects.[14] Figure 5a and Figure 5b illustrate the luminescence processes of $(C_9NH_{20})_9[Pb_3Br_{11}](MBr_4)_2$ and $(C_9NH_{20})_9[Pb_3Cl_{11}](MCl_4)_2$, respectively. When electrons are excited to the excited states (ES), strong electron-phonon coupling leads to the reorganization of the excited state structure, thereby the STEs is formed and then transit to the ground state (GS) to complete the luminescent process. The different ES of $[Pb_3Br_{11}]^{5-}$ and $[Pb_3Cl_{11}]^{5-}$ caused by the influence of halogens result in the distinct STEs and eventually showed the difference in the E_{PL}. Figure 5c shows the draft of the role of each two building parts in the luminescence processes, which $[Pb_3X_{11}]$ unit act as the main character that produces yellow/green fluorescence while $[MX_4]^{2-}$ (M = Co, Ni, Fe, Cu) unit can partly or fully quench the luminescence due to their strong self-absorption. Accordingly, the CIE diagram marked all title compounds is shown in Figure 5c to finely distinguish their luminescent colors. The specific CIE value along with the main optical parameters are listed in Table 1, all of which are consistent with our proposed model. The above optical properties with high PLQY and broad-band emssion characteristics indicate that this type materials are promising to applied in white light-emitting devices as a yellow/green component.

3. Conclusion

In summary, by introducing a new design principle for the discovery of new 0D materials with different optical building units, we successfully obtained a series 0D OIHMH $(C_9NH_{20})_9[Pb_3X_{11}](MX_4)_2$ (X = Br, Cl, M = Mn, Fe, Co, Ni, Cu, Zn), featuring two distinct anionic polyhedrons named $[Pb_3X_{11}]^{5-}$ and $[MX_4]^{2-}$. The different absorption of $[MX_4]^{2-}$ in the visible light region endows the materials different body colors, while the STEs of $[Pb_3X_{11}]^{5-}$ lead to the yellow/green broad-band emission. By carefully analyzing the spectral data, we summarize the effects of X-position anions and M-position cations on luminescence process and finally propose a reasonable luminescence mechanism. This new type 0D OIHMH with multi-polyhedral structure provides a new direction for the design of new 0D materials and is expected to be applied in the field of other multifunctional materials.

Experimental Section

Materials and Preparation: Manganese (II) bromide ($MnBr_2$) (99.9%), Nickel (II) bromide (99.9%), Cupric (II) bromide (99.95%), Zinc (II) bromide (99.9%), Manganese (II) chloride ($MnCl_2$) (99.99%), Iron (II) chloride (99.5%), Cobalt (II) chloride (99.7%) , Cupric (II) chloride (99.99%), Zinc (II) chloride (99.99%), Lead bromide (99%), Lead chloride (99.99%), 1-buty-1-methylpyrrolidinium bromide ($C_9NH_{20}Br$) (99%), 1-buty-1-methylpyrrolidinium chloride ($C_9NH_{20}Cl$) (99%) and N, N-Dimethylformamide (DMF) (99.9%) were purchased from Aladdin Co. Ltd. (Shanghai, China). Iron (II) bromide (98%), Cobalt (II) bromide (97%) and Nickel (II) chloride (99%) were purchased from Energy Chemical. (Shanghai, China)**.** $(C_9NH_{20})_9[Pb_3X_{11}](MX_4)_2$ (X = Br, Cl, M = Mn, Fe, Co, Ni, Cu, Zn) single crystals

were synthesized as follows: 4.5 mmol of $C_9NH_{20}Br$/ $C_9NH_{20}Cl$, 1.0 mmol of MX_2 and 1.5 mmol of PbX_2 were dissolved in 1.5 mL of DMF under heating and continuous stirring at 323 K. Yellow crystals were obtained by slowly cooling the saturated solution to room temperature with the controlled cooling rate to obtain the crystals with different sizes. All chemicals were used as received from the venodrs without further purification.

Characterization: The diffraction patterns were collected from single crystals of $(C_9NH_{20})_9[Pb_3X_{11}](MX_4)_2$ (X = Br, Cl, M = Mn, Fe, Co, Ni, Cu, Zn) at 296 K using the SMART APEX II X-ray single crystal diffractometers (Bruker AXS, analytical equipment of Krasnoyarsk Center of collective use of SB RAS) equipped with a CCD-detector, graphite monochromator and Mo Kα radiation source. The absorption corrections were applied using the SADABS program. The structures were solved by the direct methods using package SHELXS and refined using the SHELXL program.[15] All hydrogen atoms were linked with C,N atoms and positioned geometrically as riding on their parent atoms with $U_{iso}(H) = U_{eq}(C,N)$. The DIAMOND program [16] is used for the crystal structure plotting. Powder X-ray diffraction (PXRD) data of $(C_9NH_{20})_9[Pb_3X_{11}](MX_4)_2$ (X = Br, Cl, M = Mn, Fe, Co, Ni, Cu, Zn) was obtained using diffractometer D8 ADVANCE (Bruker) equipped by a VANTEC detector with a Ni filter. The measurements were made using Cu Kα radiation. The structural parameters defined by single crystal analysis were used as a basic in powder pattern Rietveld refinement. The refinement was produced using TOPAS 4.2 software.[17] Thermogravimetric analysis (TGA) were performed on a

Setaram Labsys Evo at 10 ^{o}C min^{-1} in an argon flow from room temperature to 800 ^{o}C. The diffuse reflection spectra were measured on a UV-Vis-NIR spectrophotometer (SHIMADZU UV-3600) supplied with an integrating sphere. The photoluminescence excitation (PLE) and emission (PL) spectra at room temperature were recorded by an Edinburgh FLS920 fluorescence spectrophotometer with the Xe900 lamp as the excitation source. The PLQY was measured using the integrated sphere on the same FLS920 instrument, and white $BaSO_4$ powder was used as a reference to measure the absorption. The luminescence decay curves were obtained by the FLS920 using an nF900 and μF900 flash lamp and as the excitation source. The power-dependent photoluminescence spectra were measured using the 375 nm (LE-LS-375-140TFCA, 1~140mW) laser.

Supporting Information

Supporting Information is available from the Wiley Online Library or from the author.

Acknowledgements

This work is supported by the National Natural Science Foundation of China (Nos. 51722202 and 51972118), Fundamental Research Funds for the Central Universities (D2190980), the Guangdong Provincial Science & Technology Project (2018A050506004).

Received: ((will be filled in by the editorial staff))
Revised: ((will be filled in by the editorial staff))
Published online: ((will be filled in by the editorial staff))

References

[1] a) Z. Song, J. Zhao, Q. Liu, *Inorg. Chem. Front.* **2019** DOI: 10.1039/c9qi00777f; b) D. B. Mitzi, *J Chem. Soc. Dalton.* **2001**, 1-12; c) B. Saparov, D. B. Mitzi, *Chem. Rev.* **2016**, 116, 4558-4596; d) Y. Zhao, K. Zhu, *Chem. Soc. Rev.* **2016**, 45, 655-689. e) K. Chen, L. Li, *Adv. Mater.* **2019**, 31, 1901115.

[2] a) L. Mao, W. Ke, L. Pedesseau, Y. Wu, C. Katan, J. Even, M. R. Wasielewski, C. C. Stoumpos, M. G. Kanatzidis, *J Am. Chem. Soc.* **2018**, 140, 3775-3783; b) M. D. Smith, A. Jaffe, E. R. Dohner, A. M. Lindenberg, H. I. Karunadasa, *Chem. Sci.* **2017**, 8, 4497-4504.

[3] a) H. Lin, C. Zhou, Y. Tian, T. Siegrist, B. Ma, *ACS Energy Letters* **2017**, 3, 54-62; b) V. Morad, Y. Shynkarenko, S. Yakunin, A. Brumberg, R. D. Schaller, M. V. Kovalenko, *J Am. Chem. Soc.* **2019**, 141, 9764-9768.

[4] a) R. Zhang, X. Mao, Y. Yang, S. Yang, W. Zhao, T. Wumaier, D. Wei, W. Deng, K. Han, *Angew. Chem.* **2019**, 58, 2725-2729. b) C. Zhou, H. Lin, J. Neu, Y. Zhou, M. Chaaban, S. Lee, M. Worku, B. Chen, R. Clark, W. Cheng, J. Guan, P. Djurovich, D. Zhang, X. Lü, J. Bullock, C. Pak, M. Shatruk, M.-H. Du, T. Siegrist, B. Ma, *ACS Energy Letters* **2019**, 4, 1579-1583. c) M. Li, J. Zhou, G. Zhou, M. S. Molokeev, J. Zhao, V. Morad, M. V. Kovalenko, Z. Xia, *Angew. Chem.* **2019** DOI: 10.1002/anie.201911419.

[5] a) S. Yakunin, B. M. Benin, Y. Shynkarenko, O. Nazarenko, M. I. Bodnarchuk, D. N. Dirin, C. Hofer, S. Cattaneo, M. V. Kovalenko, *Nat. Mater.* **2019**, 18, 846-852; b) C. Zhou, H. Lin, Y. Tian, Z. Yuan, R. Clark, B. Chen, L. J. van de Burgt, J. C. Wang, Y. Zhou, K. Hanson, Q. J. Meisner, J. Neu, T. Besara, T. Siegrist, E. Lambers, P. Djurovich, B. Ma, *Chem. Sci.* **2018**, 9, 586-593; c) M. D. Smith, B. L. Watson, R. H. Dauskardt, H. I. Karunadasa, *Chem. Mater.* **2017**, 29, 7083-7087.

[6] a) Sakisaka Y, Ishii T, Sagawa T. *J Phys. Soc. Jpn.* **1974**, 36(5), 1365-1371; b) Ronda C R, Siekman H H, Haas C. *Physica B+ C*, **1987**, 144(3), 331-340; c) C. Liu, Z. Xia, M. Chen, M. S. Molokeev, Q. Liu, *Inorg. Chem.* **2015**, 54, 1876-1882.

[8] a) L. Mao, P. Guo, M. Kepenekian, I. Hadar, C. Katan, J. Even, R. D. Schaller, C. C. Stoumpos, M. G. Kanatzidis, *J Am. Chem. Soc.* **2018**, 140, 13078-13088. b) C. Zhou, H. Lin, M.Worku, J. Neu, Y. Zhou, Y. Tian, S. Lee, P. Djurovich, T. Siegrist, B. Ma, *J. Am. Chem. Soc.* **2018**, 140, 13181‑13184.

[9] S. Li, J. Luo, J. Liu, J. Tang, *J. Phys. Chem. Lett.* **2019**, 10, 1999-2007.

[10] a) K. E. Lawson, *J Chem. Phys.* **1967**, 47, 3627-3633; b) Y. Rodríguez-Lazcano, L. Nataf, F. Rodríguez, *Phys. Rev. B* **2009**, 80, 085115; c) M. Li, J. Zhou, M. S. Molokeev, X. Jiang, Z. Lin, J. Zhao, Z. Xia, *Inorg. Chem.* **2019**, 58, 13464−13470.

[11] a) R. Gautier, M. Paris, F. Massuyeau, *J Am. Chem. Soc.* **2019**, 141, 12619-12623; b) X. Li, P. Guo, M. Kepenekian, I. Hadar, C. Katan, J. Even, C. C. Stoumpos, R. D. Schaller, M. G. Kanatzidis, *Chem. Mater.* **2019**, 31, 3582-3590.

[12] a) P.W.M.Jacobs, *J. Phys. Chem. Solids* **1991**, *52*, 35-67. b) K. M. McCall, C. C. Stoumpos, S. S. Kostina, M. G. Kanatzidis, B. W. Wessels, *Chem. Mater.* **2017**, *29*, 4129-4145.

[13] J. Zhou, M. Li, L. Ning, R. Zhang, M. S. Molokeev, J. Zhao, S. Yang, K. Han, Z. Xia, *J. Phys. Chem. Lett.* **2019**, 10, 1337-1341.

[14] T. Hu, M. D. Smith, E. R. Dohner, M. J. Sher, X. Wu, M. T. Trinh, A. Fisher, J. Corbett, X. Y. Zhu, H. I. Karunadasa, A. M. Lindenberg, *J. Phys. Chem. Lett.* **2016**, 7, 2258-2263.

[15] G. M. Sheldrick, *Acta Cryst*. **2008**, 64, 112-122.

[16] K. Brandenburg, M. Berndt, Postfach 1251, D-53002 Boon. 2004.

[17] V. Topas, Bruker AXS: Karlsruhe, Germany. **2008**.

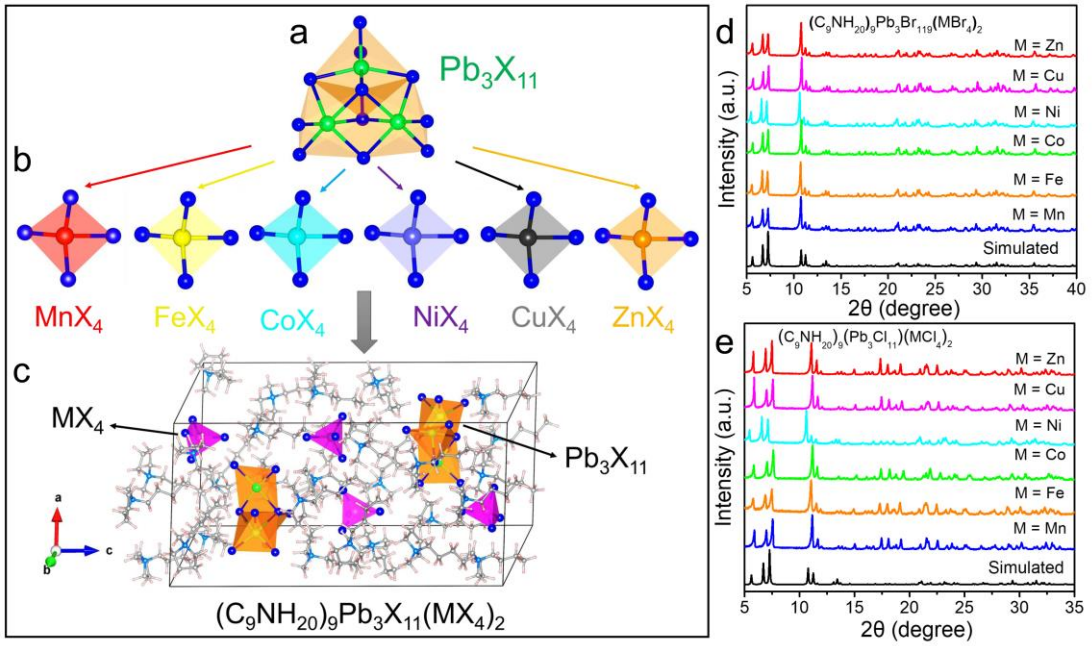

Figure 1. (a-c) The proposed structural design principle of $(C_9NH_{20})_9[Pb_3X_{11}](MX_4)_2$ (X = Br, Cl, M = Mn, Fe, Co, Ni, Cu, Zn) highlighting the local structure of $[Pb_3X_{11}]^{5-}$ block (a), $[MX_4]^{2-}$ block with different M-position cations (b) and the asymmetric part of $(C_9NH_{20})_9[Pb_3X_{11}](MX_4)_2$ unit cell (c). (d) The simulated and experimental X-ray powder patterns of $(C_9NH_{20})_9[Pb_3Br_{11}](MBr_4)_2$ (M = Mn, Fe, Co, Ni, Cu, Zn). (e) The simulated and experimental X-ray powder patterns of $(C_9NH_{20})_9[Pb_3Cl_{11}](MCl_4)_2$ (M = Mn, Fe, Co, Ni, Cu, Zn).

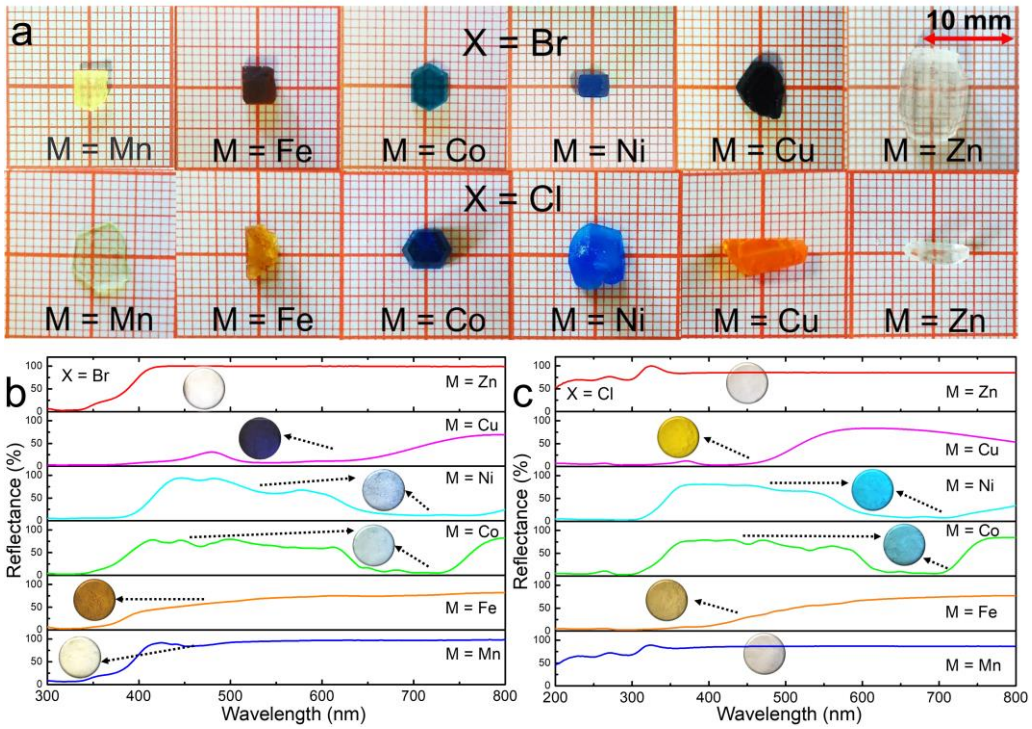

Figure 2. (a) Optical photographs of as-grown $(C_9NH_{20})_9[Pb_3X_{11}](MX_4)_2$ (X = Br, Cl, M = Mn, Fe, Co, Ni, Cu, Zn) crystals in the daylight. (b) and (c) UV-Vis diffuse

reflectance spectra of $(C_9NH_{20})_9[Pb_3X_{11}](MX_4)_2$ powder samples. Inset: Optical photographs of powder samples under day light.

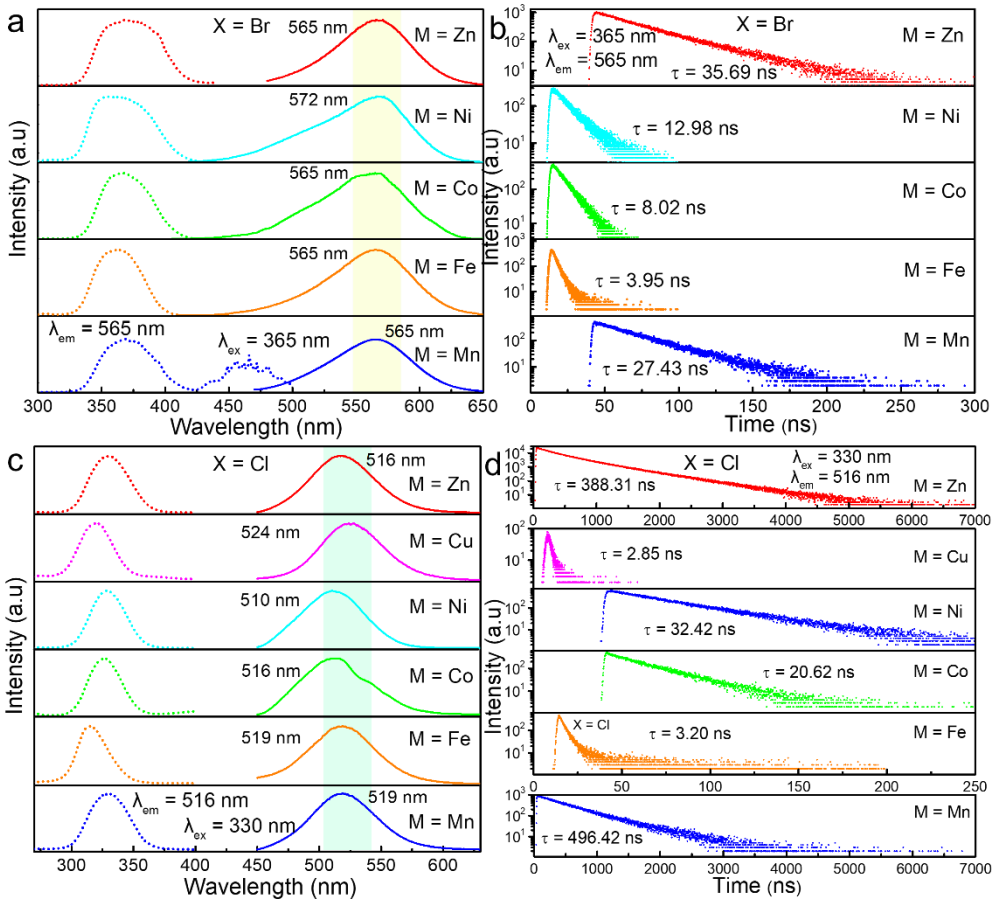

Figure 3. (a) PLE and PL spectra of $(C_9NH_{20})_9[Pb_3Br_{11}](MBr_4)_2$ (M = Mn, Fe, Co, Ni, Zn) upon excitation of 365 nm and different monitoring wavelength about 565 nm. (b) The room temperature photoluminescence decay curves of $(C_9NH_{20})_9[Pb_3Br_{11}](MBr_4)_2$ crystals monitored the emission at 565 nm upon excitation of 365 nm. (c) PLE and PL spectra of $(C_9NH_{20})_9[Pb_3Cl_{11}](MCl_4)_2$ (M = Mn, Fe Co, Ni, Cu, Zn) upon excitation of 330 nm and different monitoring wavelength about 516 nm. (d) The room temperature photoluminescence decay curves of $(C_9NH_{20})_9[Pb_3Cl_{11}](MCl_4)_2$ crystals monitored the emission at 516 nm upon excitation of 330 nm.

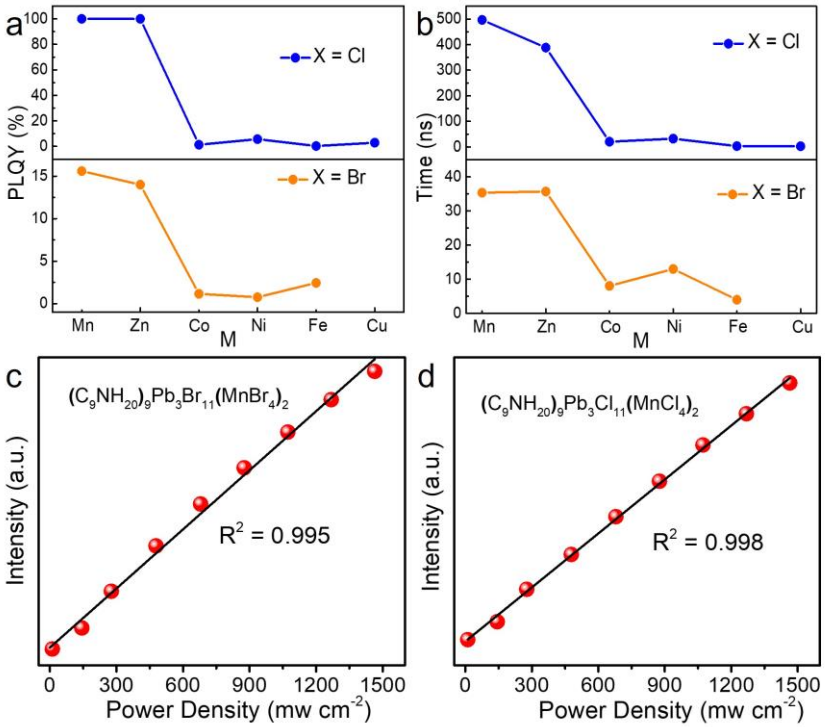

Figure 4. (a) Variations of the PLQY of $(C_9NH_{20})_9[Pb_3Br_{11}](MBr_4)_2$ (M = Mn, Fe, Co, Ni, Zn) and $(C_9NH_{20})_9[Pb_3Cl_{11}](MCl_4)_2$ (M = Mn, Fe Co, Ni, Cu, Zn) with different M-position cations. (b) Variations of the photoluminescence decay time of $(C_9NH_{20})_9[Pb_3X_{11}](MX_4)_2$ with different M-position cations. (c) and (d) the emission intensities at 565 nm excited at 375 nm as a function of the excitation power density of the selected sample of $(C_9NH_{20})_9Pb_3Br_{11}(MnBr_4)_2$ and $(C_9NH_{20})_9Pb_3Cl_{11}(MnCl_4)_2$, respectively.

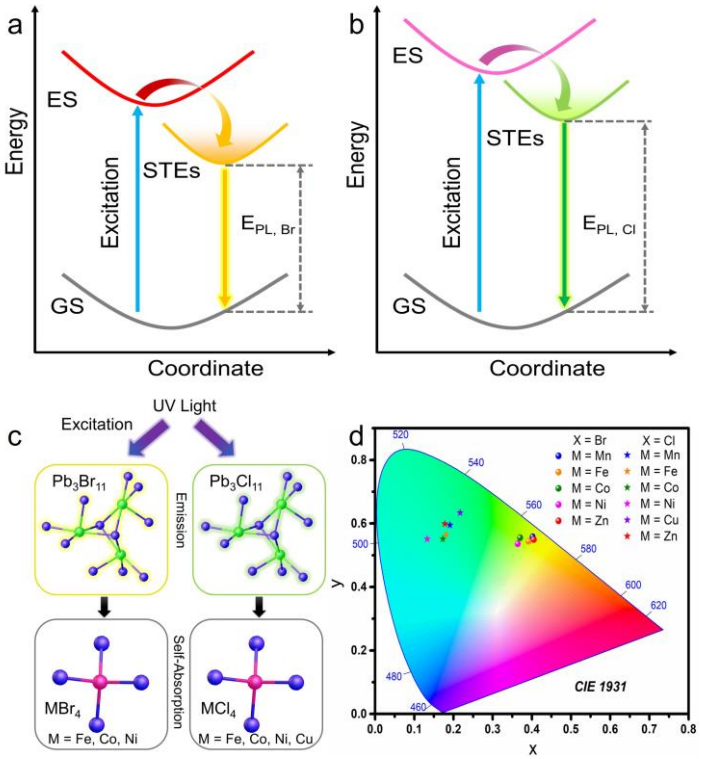

Figure 5. Schematic diagram of luminescence processes originting from $[Pb_3Br_{11}]$ part (a) and $[Pb_3Cl_{11}]^{5-}$ part (b), GS = groud state, ES = Excitation state, E_{PL} = emission energy. (c) Proposed models and differences suggesting the photoluminescence and self-absorption of $(C_9NH_{20})_9[Pb_3X_{11}](MX_4)_2$.(d) CIE chromaticity diagram of $(C_9NH_{20})_9[Pb_3X_{11}](MX_4)_2$ crystals.

Table 1. Summary of luminescence properties parameters of $(C_9NH_{20})_9[Pb_3Br_{11}](MBr_4)_2$ (M = Mn, Fe, Co, Ni, Zn) and $(C_9NH_{20})_9[Pb_3Cl_{11}](MCl_4)_2$ (M = Mn, Fe Co, Ni, Cu, Zn) with excitation wavelength of 365 nm.

Compound	FWHM (nm)	PLQY (%)	Lifetime (ns)	CIE (x,y)
$(C_9NH_{20})_9[Pb_3Br_{11}](MnBr_4)_2$	75	15.6	35.35	(0.402,0.558)
$(C_9NH_{20})_9[Pb_3Br_{11}](FeBr_4)_2$	76	2.44	3.95	(0.392,0.544)
$(C_9NH_{20})_9[Pb_3Br_{11}](CoBr_4)_2$	81	1.16	8.02	(0.370,0.555)
$(C_9NH_{20})_9[Pb_3Br_{11}](NiBr_4)_2$	84	0.76	12.98	(0.364,0.536)
$(C_9NH_{20})_9[Pb_3Br_{11}](ZnBr_4)_2$	69	13.9	35.69	(0.405,0.549)
$(C_9NH_{20})_9[Pb_3Cl_{11}](MnCl_4)_2$	61	~100	496.42	(0.191,0.595)
$(C_9NH_{20})_9[Pb_3Cl_{11}](FeCl_4)_2$	63	0.31	3.20	(0.181,0.565)
$(C_9NH_{20})_9[Pb_3Cl_{11}](CoCl_4)_2$	66	1.32	20.62	(0.173,0.551)
$(C_9NH_{20})_9[Pb_3Cl_{11}](NiCl_4)_2$	60	5.71	32.42	(0.133,0.551)
$(C_9NH_{20})_9[Pb_3Cl_{11}](CuCl_4)_2$	59	2.89	2.85	(0.217,0.634)
$(C_9NH_{20})_9[Pb_3Cl_{11}](ZnCl_4)_2$	61	~100	388.31	(0.178,0.599)

Table of Contents entry

We propose a universal design principle toward 0D hybrid metal halides built from two distinct units with different optical functions, and further expanding this family by equivalent cation substitution and halogen replacement. $(C_9NH_{20})_9[Pb_3X_{11}](MX_4)_2$ (X = Br, Cl, M = Mn, Fe, Co, Ni, Cu, Zn) comprising optical active centers of $[Pb_3X_{11}]^{5-}$ and $[MX_4]^{2-}$, were successfully synthesised. Interestingly, the body colors varies with the different crystals, covering almost the entire visible light region. These crystals show broad-band yellow/green emission under UV excitation, ascribed to the STEs of $[Pb_3X_{11}]^{5-}$ cluster. The design principle of such dual-functional units opens a new door for expolring multifuctional applications of 0D materials.

Keyword: Hybrid metal halides; Structural design; Optical functional applications

Mingze Li, Jun Zhou, Maxim S. Molokeev, Jing Zhao, Zhiguo Xia*

Optical Functional Units in Zero-Dimentional Metal Halides as a Paradigm of Tunable Photoluminescence and Multi-Component Chromophores

TOC

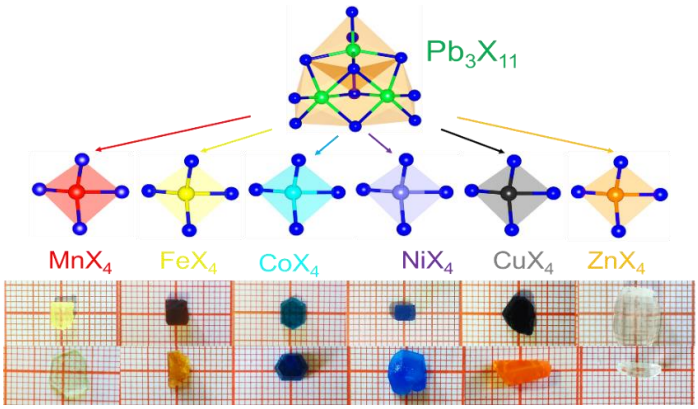
Pb_3X_{11}
MnX_4
FeX_4
CoX_4
NiX_4
CuX_4
ZnX_4

Supporting Information

Optical Functional Units in Zero-Dimentional Metal Halides as a Paradigm of Tunable Photoluminescence and Multi-Component Chromophores

Mingze Li, Maxim S. Molokeev, Jing Zhao, Zhiguo Xia*

Table S1. The crystal structure parameters of $(C_9NH_{20})_9[Pb_3X_{11}](MX_4)_2$.

Formula moiety	$(C_9NH_{20})_9Pb_3Br_{11}(MBr_4)_2$			
	M = Mn	M = Fe	M = Co	M = Ni
Molecular weight	3485.61	3389.52	3526.71	3431.15
Temperature (K)	296	296	296	296
Space group, Z	P31c, 2	P31c, 2	P31c, 2	P31c, 2
a (Å)	15.2197 (7)	15.2112 (14)	15.2024(16)	15.1953 (19)
c (Å)	31.4623 (16)	31.389 (3)	31.352 (3)	31.357 (4)
V (Å^3)	6311.5 (7)	6289.8 (13)	6275.2 (15)	6270.3 (18)
ρcalc (g/cm^3)	1.834	1.79	1.849	1.84
2 $_{max}$ (°)	52.8	46.56	46.49	46.68
R1 [F_o > 4σ(F_o)]	0.0798	0.0884	0.0787	0.0856
wR2	0.2179	0.2415	0.2299	0.2345
Goof	1.018	1.102	1.418	1.073

Formula moiety	$(C_9NH_{20})_9Pb_3Br_{11}(MBr_4)_2$	$(C_9NH_{20})_9Pb_3Cl_{11}(MCl_4)_2$		
	M = Zn	M = Mn	M = Zn	M = Co
Molecular weight	3437.36	2602.77	2670.74	2635.21
Temperature (K)	296	296	296	296
Space group, Z	P31c, 2	P31c, 2	P31c, 2	P31c, 2
a (Å)	15.1897 (9)	14.918 (3)	15.074 (6)	14.8513 (15)
c (Å)	31.3901 (18)	30.735 (7)	31.053 (13)	30.717 (3)

V (Å^3)	6272.2 (8)	5923 (3)	6111 (6)	5867.4 (13)
ρcalc (g/cm^3)	1.82	1.459	1.441	1.513
2 $_{max}$ (°)	52.84	54.3	46.4	51.4
R1 [F_o > 4σ(F_o)]	0.0801	0.0759	0.0735	0.0727
wR2	0.2194	0.2517	0.231	0.2223
Goof	0.999	1.138	1.116	0.966

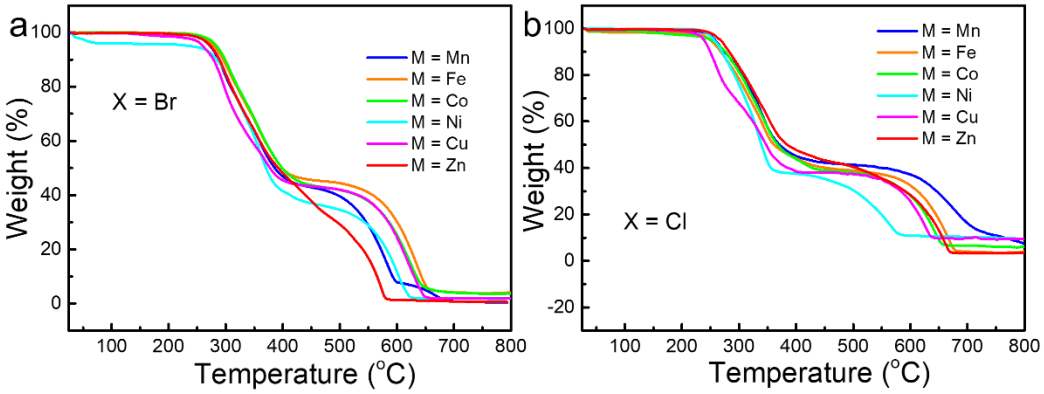

Figure S1. TGA data of $(C_9NH_{20})_9[Pb_3Br_{11}](MBr_4)_2$ (M = Mn, Fe, Co, Ni, Zn) and $(C_9NH_{20})_9[Pb_3Cl_{11}](MCl_4)_2$ (M = Mn, Fe Co, Ni, Cu, Zn).

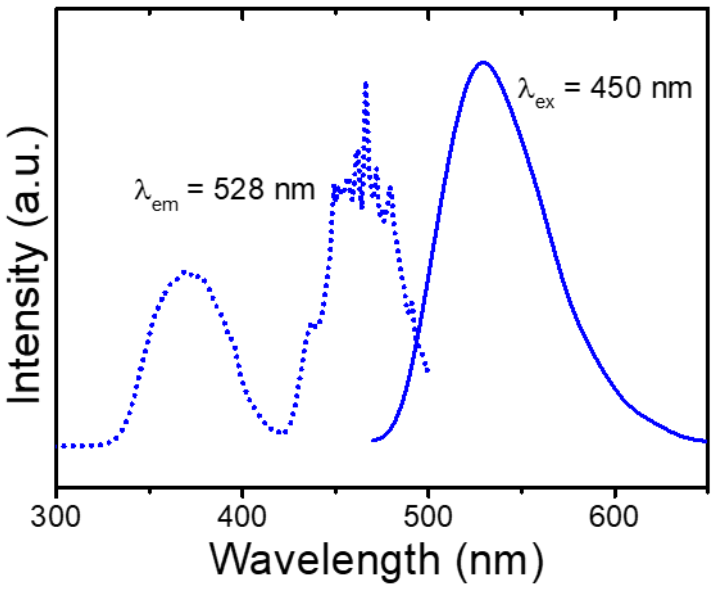

Figure S2. PL and PLE spectra of $(C_9NH_{20})_9[Pb_3Br_{11}](MnBr_4)_2$ monitored at excitation wavelength of 450 nm and emission wavelength of 528 nm.

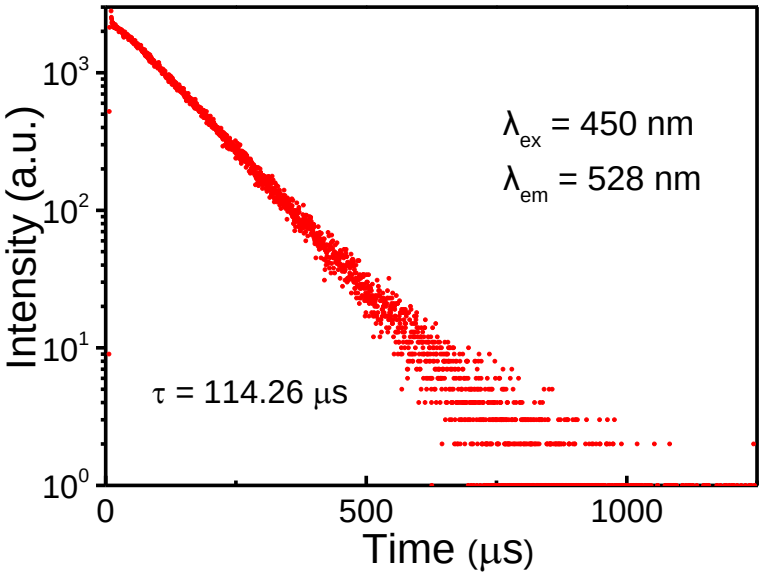

Figure S3. Room-temperature PL decay curves of $(C_9NH_{20})_9[Pb_3Br_{11}](MnBr_4)_2$ monitored at 528 nm and excited at 450 nm.

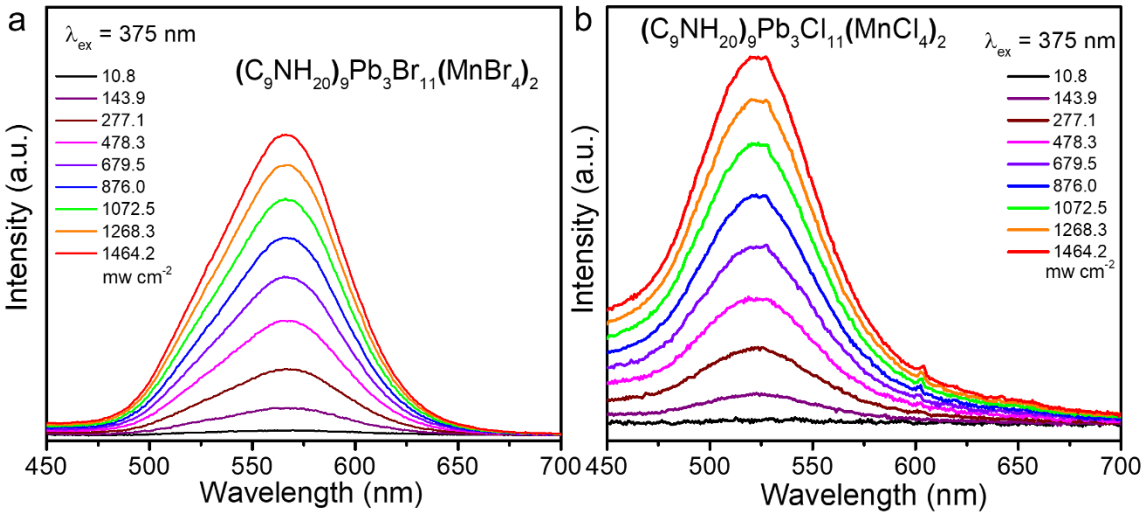

Figure S4. Excitation power dependent PL spectra of $(C_9NH_{20})_9[Pb_3Br_{11}](MnBr_4)_2$ and $(C_9NH_{20})_9[Pb_3Cl_{11}](MnCl_4)_2$ excited at 375 nm.